A Discontinuous Galerkin Scheme for Transient Multiphysics Simulation of Organic Electrochemical Transistors

A Discontinuous Galerkin Scheme for Transient Multiphysics Simulation of Organic Electrochemical Transistors

Ming Dong, Liang Chen, and Hakan Bagci
Electrical and Computer Engineering Program
Computer, Electrical and Mathematical Science and Engineering Division
King Abdullah University of Science and Technology (KAUST), Thuwal, 23955-6900, Saudi Arabia
{ming.dong, liang.chen, hakan.bagci}@kaust.edu.sa

Abstract

A time domain discontinuous Galerkin (DGTD)-based framework is developed to analyze three-dimensional organic electrochemical transistors (OECTs). The proposed framework uses a local DG scheme to discretize the (non-linearly) coupled system of the Poisson equation (in electric potential) and the drift-diffusion (DD) equations (in charge densities) in space. To reduce the computational requirements, a dual-mesh scheme, which uses a dense mesh for the DD equations and a much coarser mesh for the Poisson equation, is used. Furthermore, an implicit-explicit time integration scheme, which allows for a significantly larger time-step size, is utilized to efficiently account for the extremely long response time of OECTs. Numerical results are provided to demonstrate the applicability and accuracy of the proposed solver.

I. Introduction

Organic electrochemical transistors (OECTs), which support a channel that allows for both ionic and electronic conduction, have demonstrated exceptional performance in numerous applications such as logic circuits, neuromorphic elements, and bioelectronics [1]. Numerical methods capable of simulating OECTs are essential in their design and optimization. To this end, several schemes have been proposed, but it is hard to find one that can be satisfactorily used in industrial problems.

The time domain discontinuous Galerkin (DGTD) method [2], as a hybrid method between time domain finite volume method (TDFVM) and time domain finite element method (TDFEM), is equipped with several advantages: The mesh can be non-conformal, it allows for easier implementations of h- and/or p-adaptive mesh refinement techniques, and it is easy to parallelize. These properties make DGTD an attractive option for multiphysics simulations, and indeed, it has been used to simulate semiconductor devices [3], [4].

In this work, a DGTD-based framework is proposed to simulate three-dimensional (3D) transient response of OECTs. The proposed framework uses a local DG (LDG) scheme to discretize the (non-linearly) coupled system of the Poisson equation (in electric potential) and the drift-diffusion (DD) equations (in charge densities) in space [5]. The resulting semi-discretized matrix equation is integrated in time using an implicit-explicit (IMEX) scheme [6]. This scheme uses a significantly larger time-step size (compared to fully explicit scheme) and helps to efficiently

account for the extremely long response time of OECTs ($\sim 1\,\mathrm{ms}$). To further reduce the computational requirements of the proposed framework, a dual mesh scheme, where the Poisson equation is discretized on a coarser mesh and the DD equations are discretized on a finer mesh, is used. This dual mesh scheme uses a simple interpolation to establish the "connection" between two different mesh systems and significantly reduces the computational cost of solving the Poisson equation at each time step.

II. Formulation

The (nonlinearly) coupled system of Poisson and DD equations describes the space- and time-dependent behavior of carriers and electric field inside the OECT devices. This coupled system reads [5]:

$$\nabla \cdot [\varepsilon(\mathbf{r})\mathbf{E}(\mathbf{r},t)] = e[n_{\mathrm{h}}(\mathbf{r},t) + n_{\mathrm{c}}(\mathbf{r},t) - n_{\mathrm{a}}(\mathbf{r},t) - N_{\mathrm{A}}] \tag{1}$$

$$\mathbf{E}(\mathbf{r},t) = -\nabla\phi(\mathbf{r},t) \tag{2}$$

$$\begin{aligned}\partial_t n_{\mathrm{s}}(\mathbf{r},t) = &- \nabla \cdot [z_{\mathrm{s}}\mu_{\mathrm{s}}(\mathbf{r})n_{\mathrm{s}}(\mathbf{r},t)\mathbf{E}(\mathbf{r},t)] \\ &+ \nabla \cdot [D_{\mathrm{s}}(\mathbf{r})\mathbf{q}_{\mathrm{s}}(\mathbf{r},t)]\end{aligned} \tag{3}$$

$$\mathbf{q}_{\mathrm{s}}(\mathbf{r},t) = \nabla n_{\mathrm{s}}(\mathbf{r},t) \tag{4}$$

where $\varepsilon(\mathbf{r})$ is permittivity, $\mathbf{E}(\mathbf{r},t)$ is the electric field, $\phi(\mathbf{r},t)$ is the electric potential, e is the electron charge, N_{A} is the density of ionized acceptors, $n_{\mathrm{h}}(\mathbf{r},t)$, and $n_{\mathrm{c}}(\mathbf{r},t)$ and $n_{\mathrm{a}}(\mathbf{r},t)$ are the carrier densities of cation, anion and hole, respectively. In (3) and (4), $\mathrm{s} \in \{\mathrm{h},\mathrm{c},\mathrm{a}\}$, $z_{\mathrm{h}} = z_{\mathrm{c}} = 1$, $z_{\mathrm{a}} = -1$ indicate the relative charge of different carriers, $\mu_{\mathrm{s}}(\mathbf{r})$ and $D_{\mathrm{s}}(\mathbf{r})$ represent the carrier mobility and diffusion coefficient, respectively, and $\mathbf{q}_{\mathrm{s}}(\mathbf{r},t)$ is an auxiliary variable introduced to reduce the order of spatial derivative on carrier density.

To facilitate the numerical solution, the computation domain is divided into N non-overlapping tetrahedrons and the system (1)-(4) is spatially discretized using the local DG method. This leads to the semi-discretized matrix system:

$$\begin{bmatrix} 0 & \bar{\varepsilon}\bar{D} \\ \bar{G} & \bar{M} \end{bmatrix} \begin{bmatrix} \bar{\Phi} \\ \bar{E} \end{bmatrix} = \begin{bmatrix} \bar{B}_{\phi} \\ \bar{B}_{\mathbf{E}} \end{bmatrix} \tag{5}$$

$$\begin{bmatrix} \bar{M}_{\mathrm{h}}\partial_t + \bar{C} & -\bar{d}\bar{D} \\ -\bar{G} & \bar{M} \end{bmatrix} \begin{bmatrix} \bar{N}_{\mathrm{h}} \\ \bar{Q} \end{bmatrix} = \begin{bmatrix} \bar{B}_{n_{\mathrm{h}}} \\ \bar{B}_{\mathbf{q}} \end{bmatrix} \tag{6}$$

where $\bar{\Phi} = [\bar{\Phi}_1, ..., \bar{\Phi}_N]^T$, $\bar{E} = [\bar{E}_1^x, \bar{E}_1^y, \bar{E}_1^z, ..., \bar{E}_N^z]^T$, $\bar{N}_{\mathrm{h}} = [\bar{N}_{\mathrm{h}1}, ..., \bar{N}_{\mathrm{h}N}]^T$, and $\bar{Q} = [\bar{Q}_1^x, \bar{Q}_1^y, \bar{Q}_1^z, ..., \bar{Q}_N^z]^T$ are the vectors storing the unknown expansion coefficients of the DG discretization. $\bar{M}$ is the mass matrix and $\bar{G}$ and $\bar{D}$ represent the gradient and the divergence operators, respectively. $\bar{B}_{\phi}$, $\bar{B}_{\mathbf{E}}$, $\bar{B}_{n_{\mathrm{h}}}$ and $\bar{B}_{\mathbf{q}}$ correspond to the boundary conditions enforced on the boundary of the computation domain. Note that, for the sake of brevity, only the discretized form of the hole equations are provided here and also the detailed expressions of the operators/matrices in (5)-(6) can be found in [3], [4].

The IMEX scheme is used to efficiently integrate (6) in time. The linear diffusion term is treated implicitly (using backward Euler method) while the non-linearly coupled drift term is treated explicitly (using forward Euler method). This yields the final form of the time marching scheme as:

$$(\bar{I} - \Delta t \bar{M}_{\mathrm{h}}^{-1} \bar{d} \bar{D} \bar{M}^{-1} \bar{G}) \bar{N}_{\mathrm{h}}^{m+1} = (\bar{I} - \Delta t \bar{M}_{\mathrm{h}}^{-1} \bar{C}) \bar{N}_{\mathrm{h}}^{m} + \bar{M}_{\mathrm{h}}^{-1} \bar{N}_{\mathrm{h}}^{m} + \Delta t \bar{M}_{\mathrm{h}}^{-1} \bar{d} \bar{D} \bar{M}^{-1} \bar{B}_{\mathbf{q}} \tag{7}$$

where m is the index of the time step. This IMEX time integration permits the LDG framework to use a significantly larger Δt in the simulation (compared to fully explicit time integration schemes).

To further reduce the computational cost of the simulation, a dual (spatial) mesh scheme is applied. On the denser mesh the Poisson equation is discretized while on the coarser mesh DD equations are discretized. A simple interpolation is used to establish the "connection" between the solutions on the two meshes:

$$\mathbf{f} = \mathcal{V}^{\mathrm{I}} \mathcal{V}^{-1} \boldsymbol{\phi} \tag{8}$$

where $\boldsymbol{\phi}$ is the vector containing the solutions at the nodal points, $\mathbf{f}$ is the interpolated results at the target points, $\mathcal{V}$ and $\mathcal{V}^{\mathrm{I}}$ are the generalized Vandermonde matrices with entries $\mathcal{V}_{ij} = \tilde{P}_j(\mathbf{r}_i)$ and $\mathcal{V}^{\mathrm{I}}_{ij} = \tilde{P}_j(\mathbf{r}^{\mathrm{I}}_i)$, $\mathbf{r}_i$ and $\mathbf{r}^{\mathrm{I}}_i$ are the mapped coordinates of the nodal points and the target points in the reference element, respectively, and $\tilde{P}_j(\mathbf{r})$ is the j^{th} orthonormal polynomial basis [2], [7].

III. Numerical Examples

In this example, moving carrier front simulation described in [8] is revisited. This simulation investigates ion and hole transport in a planar junction between an electrolyte and a conducting polymer film. The geometry considered in this example is shown in Fig. 1. The device consists of a solid $175\,\mathrm{nm}$ film inserted between a $25\,\mathrm{nm}$ electrolyte (on the left) and a metal electrode (on the right). A bias voltage, which is applied between the metal electrode and an electrode immersed in the electrolyte, drives cations from electrolyte to the film and anions from film to the electrolyte. Meanwhile, the holes drift towards the metal electrode on the right. All the parameters of the 3D simulation described here are same as the 1D simulation conducted in [8]. For this simulation, the IMEX time integration scheme allows Δt to be 100 times larger than the one that would be used by a fully explicit time integration scheme.

The snapshots of hole, anion and cation densities and the electric potential at $t = 2, 4, 6, 8, 10\,\mu\mathrm{s}$ are shown in Fig. 2. The figure clearly shows that the applied bias voltage pushes the cations and holes into the film while pulls

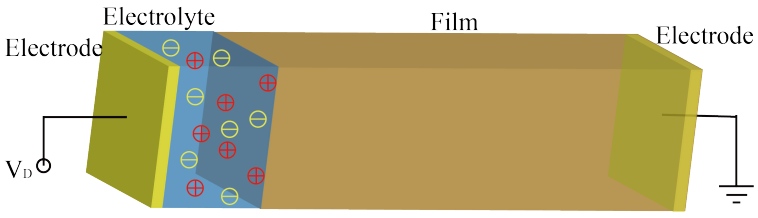

Fig. 1. Schematic representation of the OECT.

the anions back into the electrolyte. To demonstrate the "moving front" due to the drift of holes and injection of cations, the hole and the cation densities along the x-axis at $t = 2, 4, 6, 8, 10\,\mu$s are plotted in Fig. 3.

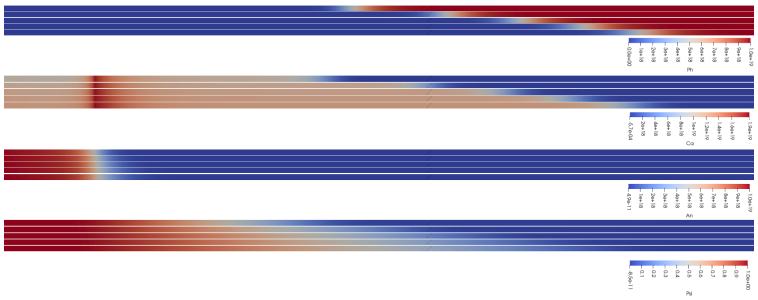

Fig. 2. Carrier densities and electric potential on the cross section of the OECT at $t = 2, 4, 6, 8, 10\,\mu$s.

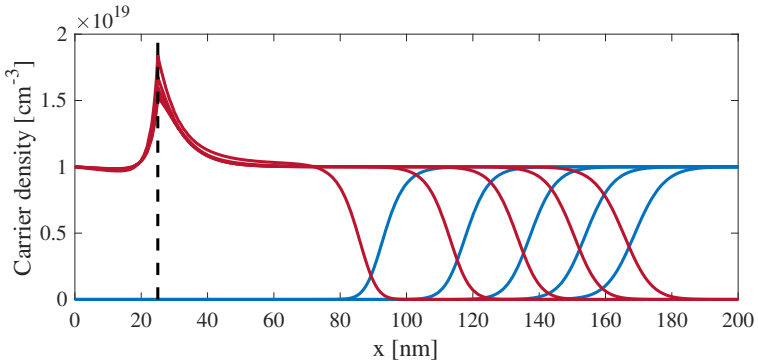

Fig. 3. "Moving front" as demonstrated by the hole and the cation densities along the x-axis at $t = 2, 4, 6, 8, 10\,\mu$s.

REFERENCES

[1] J. Rivnay, S. Inal, A. Salleo, R. M. Owens, M. Berggren, and G. G. Malliaras, "Organic electrochemical transistors," *Nat. Rev. Mater.*, vol. 3, no. 2, pp. 1–14, 2018.

[2] J. S. Hesthaven, and T. Warburton, *Nodal Discontinuous Galerkin Methods: Algorithms, Analysis, and Applications.* New York, NY, USA: Springer, 2007.

[3] L. Chen, and H. Bagci, "Seady-state simulation of semiconductor devices using discontinuous Galerkin methods," *IEEE Access*, vol. 8, pp. 16203–16215, Jan. 2020.

[4] L. Chen and H. Bagci, "Multiphysics simulation of plasmonic photoconductive devices using discontinuous Galerkin methods," *IEEE J. Multiscale Multiphys. Comput. Tech.*, vol. 5, pp. 188–200, 2020.

[5] M. Z. Szymanski, D. Tu, and R. Forchheimer, "2-D drift-diffusion simulation of organic electrochemical transistors,", *IEEE Trans. Electron Devices*, vol. 64, no. 12, pp. 5114–5120, 2017.

[6] H. Wang, C.-W. Shu, and Q. Zhang, "Stability and error estimates of local discontinuous Galerkin methods with implicit-explicit time-marching for advection-diffusion problems," *SIAM J. Numer. Anal.*, vol. 53, no. 1, pp. 206–227, 2015.

[7] L. Chen and H. Bagci, "A dual-mesh framework for multiphysics simulation of photoconductive terahertz devices," in *Proc. URSI General Assembly and Sci. Symp.*, Rome, Italy, 2020.

[8] M. Dong, L. Chen and H. Bagci, "An implicit-explicit local discontinuous Galerkin scheme for analysis of organic electrochemical transistors," in *Proc. Appl. Comput. Electromagn. Symp.*, Aug. 2021.